ARTICLE

doi:10.1038/nature11393

Distinct contribution of stem and progenitor cells to epidermal maintenance

Guilhem Mascré[1], Sophie Dekoninck[1], Benjamin Drogat[1], Khalil Kass Youssef[1], Sylvain Brohée[1,2], Panagiota A. Sotiropoulou[1], Benjamin D. Simons[3,4] & Cédric Blanpain[1,5]

The skin interfollicular epidermis (IFE) is the first barrier against the external environment and its maintenance is critical for survival. Two seemingly opposite theories have been proposed to explain IFE homeostasis. One posits that IFE is maintained by long-lived slow-cycling stem cells that give rise to transit-amplifying cell progeny, whereas the other suggests that homeostasis is achieved by a single committed progenitor population that balances stochastic fate. Here we probe the cellular heterogeneity within the IFE using two different inducible Cre recombinase–oestrogen receptor constructs targeting IFE progenitors in mice. Quantitative analysis of clonal fate data and proliferation dynamics demonstrate the existence of two distinct proliferative cell compartments arranged in a hierarchy involving slow-cycling stem cells and committed progenitor cells. After wounding, only stem cells contribute substantially to the repair and long-term regeneration of the tissue, whereas committed progenitor cells make a limited contribution.

Skin epidermis is comprised of a basal layer of proliferative cells and several suprabasal layers of terminally differentiated cells that are progressively enucleated, forming squames that are shed from the skin surface[1]. Depending on anatomical location and species, the minimum transit time from the basal layer to the cornified layer has been estimated at around 1–2 weeks[2]. In homeostasis, cells lost during the course of turnover must be perfectly compensated by cells generated in the basal layer. Different theories have been proposed to explain how this balance is achieved[1]. On the basis of morphological and proliferation studies, it has been proposed that the IFE is organized into discrete 'epidermal proliferative units' (EPUs), comprised of slow-cycling stem cells (SCs) together with around 10 transit-amplifying cell progeny, which undergo terminal differentiation after a fixed number of cell divisions[2–5]. Following the clonal marking of IFE cells by retroviruses[6–9] or mutagens[10,11], long-lived columns of labelled IFE cells that span the epidermis from the basal layer to the top of the cornified layer appear, lending support to the concept of EPUs. By contrast, the quantitative analysis of lineage tracing data in IFE using a ubiquitous promoter suggests that tissue is maintained by a single, equipotent, committed progenitor (CP) cell population in which the balance between proliferation and differentiation follows from seemingly random cell fate decisions[12,13]. Although this model is attractive in its simplicity, it does not easily explain the ability of tissue to respond rapidly to increased cell demand, such as during wound healing, and cannot rule out the presence of a quiescent or slow-cycling IFE population[14]. More importantly, whereas the contribution of different populations of hair follicle SCs to wound healing is well-established[15–18], little is known about the contribution of putative IFE SCs or CP cells to the repair of skin epidermis.

From a quantitative analysis of lineage tracing data using two different Cre recombinase–oestrogen receptor (Cre-ER) transgenic mice, we demonstrate the existence of two distinct populations of epidermal progenitors that form a SC/CP cell hierarchy that differentially contribute to the homoeostasis and repair of the epidermis.

Heterogeneity of epidermal progenitors

To probe the proliferative heterogeneity within the IFE, we made use of two Cre-ER transgenic mice that target IFE progenitors (Supplementary Fig. 1a, b). With a high dose of tamoxifen, Cre-ER under the control of the keratin 14 promoter (K14-Cre-ER) can target most cells in the basal layer of tail IFE[19]. A very low dose of tamoxifen (0.2 mg) to K14-Cre-ER/RosaYFP induced yellow fluorescent protein (YFP) expression at clonal density (Supplementary Fig. 1c). Although Cre-ER under the control of the involucrin promoter (Inv-Cre-ER) predominantly targets cells in the suprabasal layers, we have recently shown that some basal cells, characterized by K5 but not Inv protein expression, are also induced but at a lower frequency than K14-Cre-ER (Supplementary Fig. 1d–f)[20]. The basal cells marked by these two different Cre-ER comprise IFE progenitors, as demonstrated by their ability to proliferate, and give rise to differentiated progeny, forming columns of labelled cells (Supplementary Fig. 1c, d).

To determine whether the two induction protocols mark the same homogenous pool of progenitors, we first quantified their survival at different time points after tamoxifen administration. Although many of the clones induced by the K14-Cre-ER survived up to 1 year post-induction, most of the Inv-Cre-ER targeted clones were progressively lost (Fig. 1a–c). Whereas the population of 'surviving clones', defined as clones that retain at least one basal layer cell, drops by around 30% for K14 mice from 4 weeks to 6 months after labelling, the clone density falls by a factor of 10 in the Inv mice over the same period, indicating that IFE is maintained by a heterogeneous pool of progenitors with different survival potential.

Inv-Cre-ER targets committed progenitors

To gain further insight into the behaviour of these apparently distinct pools of progenitors, we quantified the pattern of growth of individual clones targeted by the Inv-Cre-ER at eight time points ranging from 3.5 days to 48 weeks post-induction, a period spanning more than half of the average lifetime of the mouse. At 3.5 days, 40% of surviving clones had undergone at least one round of cell division (Fig. 2a, b and

[1]Université Libre de Bruxelles, IRIBHM, Brussels B-1070, Belgium. [2]Université Libre de Bruxelles, Machine Learning Group, Brussels B-1050, Belgium. [3]Cavendish Laboratory, Department of Physics, J. J. Thomson Avenue, Cambridge CB3 0HE, UK. [4]The Wellcome Trust/Cancer Research UK Gurdon Institute, University of Cambridge, Tennis Court Road, Cambridge CB2 1QN, UK. [5]WELBIO, Université Libre de Bruxelles, Brussels B-1070, Belgium.

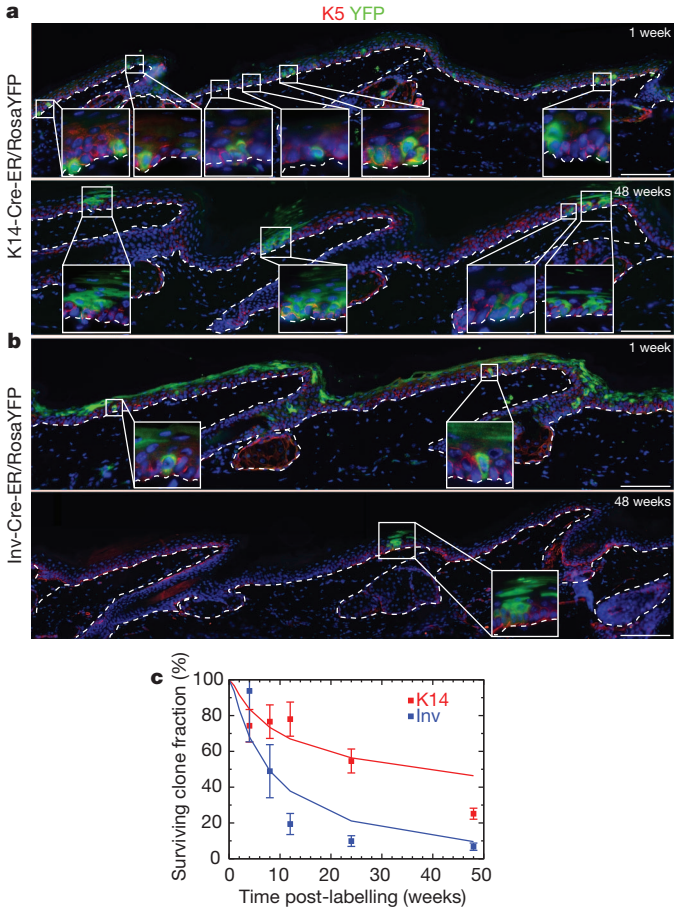

Figure 1 | K14-Cre-ER and Inv-Cre-ER target IFE progenitors with different survival characteristics. **a**, **b**, Immunostaining of K5 and YFP in K14-Cre-ER/RosaYFP (**a**) and Inv-Cre-ER/RosaYFP (**b**) tail epidermis at 1 week and 48 weeks post-induction showing the high survival rate of K14-Cre-ER clones. Dashed lines represent the basal lamina. Hoechst nuclear staining is represented in blue. **c**, Quantification of surviving clones in K14-Cre-ER/RosaYFP and Inv-Cre-ER/RosaYFP tail epidermis at different times following tamoxifen administration ($n = 327$ clones at least, for each time point of K14 and Inv). Symbols show experimental data and the lines represent the prediction of the mathematical modelling. The data has been normalized to the initial clone density as inferred by the fit to theory. Error bars show s.d. Scale bars, 200 μm.

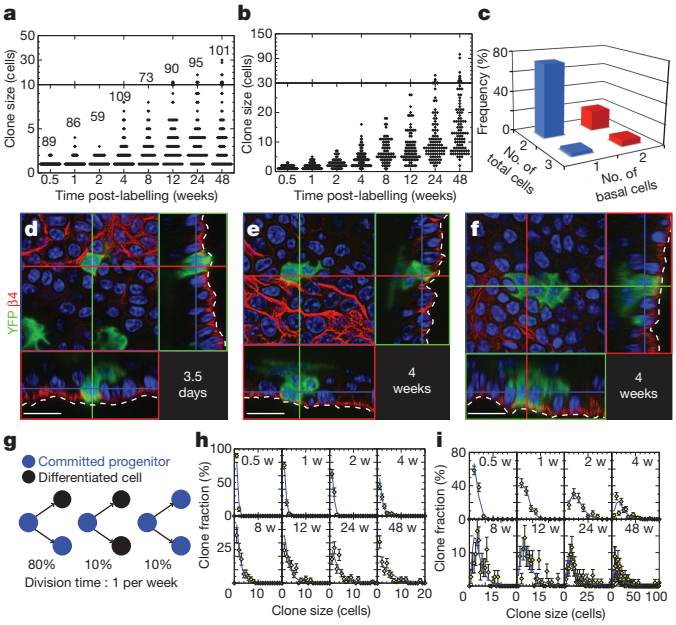

Figure 2 | Inv-Cre-ER targets IFE CP cells. **a**, **b**, Distribution of Inv-Cre-ER clone sizes as measured by basal (**a**) and total (**b**) cell content of surviving clones, imaged by confocal microscopy on whole-mount tail epidermis from 3.5 days to 48 weeks following tamoxifen administration. The number of analysed clones is indicated in **a** and this is identical in **b**, **h** and **i**. **c**, Size distribution of surviving clones with more than one cell at 3.5 days post-labelling disaggregated according to basal and total cell number ($n = 37$ clones). **d**–**f**, Confocal analysis of representative Inv-Cre-ER-targeted basal clones at 3.5 days (**d**) and 4 weeks (**e**, **f**) post tamoxifen. Dashed lines represent the basal lamina. Hoechst nuclear staining is represented in blue. **g**, A fit of the Inv-Cre-ER clonal fate data predicts that progenitors undergo population asymmetry through a combination of asymmetric cell division, symmetrical self-renewal and symmetrical differentiation with an average cell cycle time of approximately 1 week. **h**, **i**, Frequency distribution of basal (**h**) and total (**i**) clone size. Symbols represent experimental data and the lines correspond to the model prediction. Error bars show s.e.m. Scale bars, 10 μm.

Supplementary Fig. 2a), and the vast majority of these divisions resulted in one basal and one suprabasal cell (Fig. 2c, d). At 4 weeks post-induction, although almost all surviving clones had undergone at least one cell division, 40% of clones still contained only one basal cell (Fig. 2a, e), indicating that most of these divisions led to asymmetric fate outcome. However, the other 60% of surviving clones had also expanded basally (Fig. 2a, f), indicating that progenitors can also symmetrically self-renew.

This clonal heterogeneity increased progressively over the 48-week time course, indicating that progenitors follow divergent fates (Supplementary Fig. 2b, c). At the same time, the average size of surviving clones (as measured both by their total size and their 'footprint' on the basal layer) grew approximately linearly with time (Supplementary Fig. 2d), whereas the number of surviving clones progressively fell (Fig. 1c). Such behaviour mirrors that reported previously[12] in studies using a ubiquitous promoter, and indicates that Inv-Cre-ER targets the actively cycling CP cell population, in which stochastic cell loss through differentiation is perfectly compensated by duplication (Fig. 2g). This conclusion is reinforced by a quantitative analysis of the data, which confirms that the basal layer clone size distribution converges onto the hallmark scaling behaviour in which the chance of finding a clone larger than some multiple of the average stays constant over time (Supplementary Fig. 2e and Supplementary Methods, section 'Theory')[21]. From the detailed study of the basal and total clone size distribution over the 48 week time course (Fig. 2h, i, Supplementary Fig. 2f and Supplementary Methods, section 'Theory'), we are able to conclude that, following CP cell division (at an average rate of 1.21 ± 0.04 per week), 80% result in asymmetric fate (leading to one dividing and one differentiated cell) with the remainder leading to symmetric duplication or differentiation with approximately equal probability (Fig. 2g), consistent with the results from ref. 12. Indeed, from the 48 week time point, we are able to resolve a small (less than 1 in 14) bias towards terminal division.

K14-Cre-ER targets long-lived SCs

To determine whether the dynamics of K14 clones are different from the Inv clones, we performed extensive clonal analysis using the K14-Cre-ER mice ranging from 3.5 days to 48 weeks post-induction (Fig. 3). At just 3.5 days, 60% of K14 clones had already undergone one round of cell division (Fig. 3a, b and Supplementary Fig. 3a), whereas the fraction of clones involving two or more basal cells was greatly increased compared with Inv (Fig. 3a–d). However, following an initial abrupt expansion, the growth of K14 clones rapidly decelerates over the first few weeks, with the size distribution from 8 weeks to 6 months post-induction showing only a modest expansion (Fig. 3a–f and Supplementary Fig. 3a–c). Alongside the propensity of clones to persist, these observations are consistent with the K14 promoter targeting both the CP cell population and a second, slow-cycling, SC population. In particular, the precipitous expansion of clones (Fig. 3a–c), which is far more rapid than that found in the

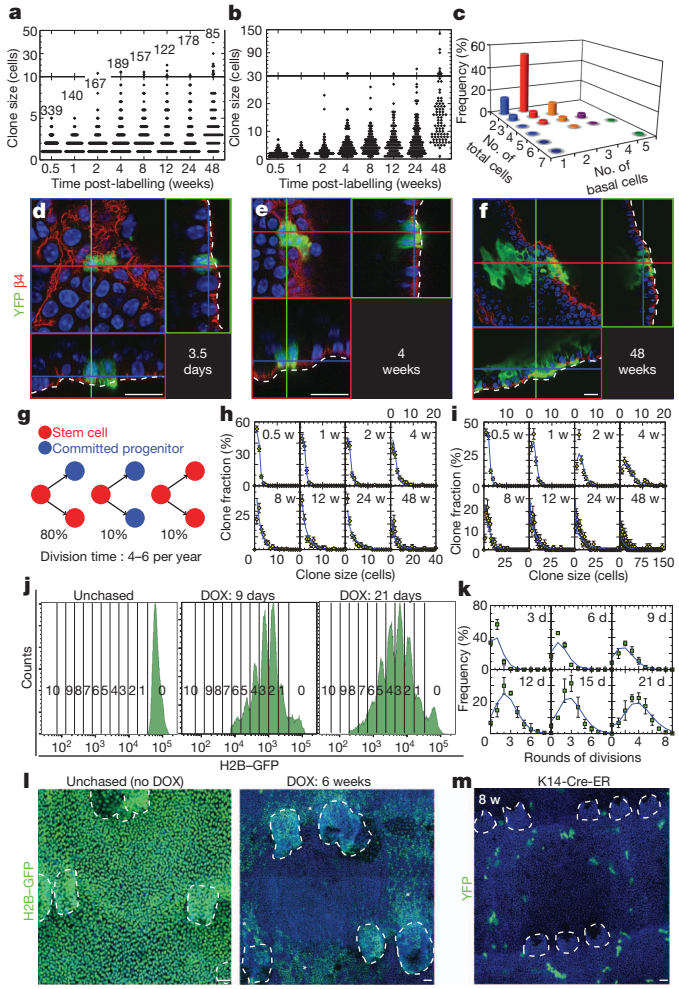

Figure 3 | K14-Cre-ER targets IFE SCs. **a**, **b**, Distribution of K14-Cre-ER clone sizes as measured by basal (**a**) and total (**b**) cell content of surviving clones, imaged by confocal microscopy on whole-mount tail epidermis from 3.5 days to 48 weeks following tamoxifen administration. The number of analysed clones is indicated in **a** and this is identical in **b**, **h** and **i**. **c**, Size distribution of surviving clones with more than one cell at 3.5 days post-labelling disaggregated according to basal and total cell number ($n = 197$ clones). **d**–**f**, Confocal analysis of representative K14-Cre-ER targeted basal clones at 3.5 days (**d**), 4 weeks (**e**) and 48 weeks (**f**) post tamoxifen. Dashed lines represent the basal lamina. Hoechst nuclear staining is represented in blue. Scale bars, 10 μm. **g**, Biophysical modelling of the clonal fate data predicts that K14-Cre-ER targets both CP cells and SCs with the latter undergoing population asymmetry through a combination of asymmetric cell division, symmetrical self-renewal and symmetric differentiation with an average cell cycle rate of between 4 and 6 per year. **h**, **i**, Frequency distribution of basal (**h**) and total (**i**) clone size. Symbols represent data and the lines correspond to the model prediction. **j**, FACS analysis of K5tTA/tet(O)-H2BGFP mice at different time point following DOX administration. **k**, Frequency of the number of cell divisions that surviving basal IFE cells undergo during the chase period as quantified by FACS analysis at different time points after DOX administration to adult K5tTA/tet(O)-H2BGFP mice. Symbols represent the average of the experimental data ($n = 3$ mice at each time point). Lines correspond to the predicted model dynamics (Supplementary Methods, section 'Theory'). **l**, **m**, Confocal analysis of H2B–GFP immunostaining in unchased mice (no DOX) (left panel) and 6 weeks after DOX administration (right panel), showing the preferential localization of the slow-cycling IFE cells in the bottom of epidermal undulations (stars) (**l**) and of YFP immunostaining in K14-Cre-ER/RosaYFP 8 weeks after tamoxifen administration (**m**). Dashed lines are hair follicles. Scale bars, 20 μm. Error bars show s.e.m. Hoechst nuclear staining is represented in blue.

Inv study (Fig. 2a–c), indicates that SCs are induced predominantly on cell cycle entry. This conclusion is consistent with the observation that, after administration of 12-*O*-tetradecanoyl phorbol-13-acetate (TPA), a drug that stimulates epidermal proliferation, there is an 80% increase in clone labelling after low dose of tamoxifen (Supplementary Fig. 4a, b). Furthermore, the deceleration in the rate of clonal expansion at subsequent times indicates that, after division, SCs re-enter a quiescent phase whereas their CP cell progeny go on to proliferate and differentiate. For these clones, the quiescent SC 'mother' provides an anchor to the basal layer (Fig. 3a–f and Supplementary Fig. 3a), leading to clonal persistence. Such behaviour is consistent with the observation that, in K14 mice, the level of positive regulators of the cell cycle, such as *Ccnb1* and *Cdc20*, decreased, whereas negative regulators of the cell cycle, such as *Cdkn1a* and *Cdkn2a*, increased in basal cells between 3.5 days and 8 weeks (Supplementary Fig. 4c–e).

With this hypothesis, if we assume that SC division can also lead to all three possible fates (Fig. 3g), the predicted model dynamics provides an excellent fit to the clone size data (basal and suprabasal) over the wide range of time points up to 1-year post-labelling (Fig. 3h, i, Supplementary Fig. 3c, d and Supplementary Methods, section 'Theory'). In particular, we find that SCs account for some 50 ± 5% of the induced proliferative cells. With a SC division rate as low as 4–6 per year, a factor of 10–20 times slower than CP cells, most of the clone size data (from 1 week to 3 months post-labelling) are largely fixed by the known characteristics of CP cells. Drawing on the early (3.5 day) time point, we are able to deduce that, in common with their progenitor cell progeny, SCs undergo population asymmetric self-renewal with some 80 ± 10% of SC divisions resulting in asymmetric fate (one SC and one CP cell), whereas the remaining divisions are equally balanced between SC duplication and symmetrical differentiation into two CPs (Fig. 3g). Finally, although the analysis points at a proliferative hierarchy, we cannot rule out the possibility that proliferative cells may switch reversibly between CP and SC behaviour if the transfer rate is sufficiently low. Moreover, the data do not allow us to infer whether the balance between SC proliferation and differentiation follows from intrinsic (cell autonomous) regulation or is controlled by environmental cues (Supplementary Methods, section 'Theory')[21].

Proliferation dynamics of the IFE

To challenge these findings, we applied further independent experimental assays to explore the IFE cell proliferation using a combination of cell cycle analysis, 5-bromo-2-deoxyuridine (BrdU) incorporation, and pulse-chase experiments using the K5tTA/tet(O)-H2B-GFP reporter mouse, that have proved useful in resolving quantitatively the proliferation dynamics of hair follicle bulge SCs[15,22–24]. We first determined the cell cycle profile of basal IFE cells by determining their DNA content. These experiments show that around 9% of $\alpha6^{+}CD34^{-}$ IFE cells were in the S/G2/M phase of the cell cycle (Supplementary Fig. 5a, b). Continuous BrdU administration labelled 28 ± 2% and 57 ± 10% of K5-expressing cells after 24 and 72 h, respectively, indicating an average cell division time of around 6 ± 1 days (Supplementary Fig. 5c, d and Supplementary Methods, section 'Theory'), consistent with the inferred CP cell division rate.

To develop a more refined method to quantify proliferation kinetics over a longer period, we used K5tTA/tet(O)-H2B-GFP mice (Supplementary Fig. 6). In the absence of doxycycline (DOX), histone 2B domain–green fluorescent protein (H2B–GFP) fusion protein is expressed at a very high level in a discrete peak of fluorescence (Supplementary Fig. 6a–c, top panels). Following DOX administration, H2B–GFP fluorescence decreases by a factor of two after cell division[15,22] (Supplementary Fig. 6a–c, bottom panels). The discrete peak of H2B–GFP fluorescence observed by fluorescence-activated cell sorting (FACS) analysis during the chase period allowed an accurate quantification of the distribution in the number of rounds of division experienced by basal layer cells ($\alpha6^{+}CD34^{-}$) at various time points following induction (Fig. 3j and Supplementary Fig. 6d). At 3 weeks post-DOX administration, dilution of H2B–GFP label shows evidence of CP cell proliferation, while a small peak at high levels of fluorescence is consistent with around 5% or less of label-retaining cells (LRCs).

From the quantification of fluorescence over the time course, the distribution of cell divisions was shown to be quantitatively consistent with the inferred SC and CP cell dynamics (Fig. 3k and Supplementary Methods, section 'Theory'). Notably, after 6 weeks of chase, the H2B–GFP label has become diluted in the vast majority of basal layer cells and only a small minority retain high levels of expression (Supplementary Fig. 6d). Intriguingly, these LRCs are localized to the bottom of the undulations of the tail epidermis (Fig. 3l), which correlate with the location of persistent clones derived by the K14 assay (Fig. 3m), and are reminiscent of the so-called rete ridges in human epidermis, where epidermal SCs were thought to reside[25,26].

Molecular characterization of SCs and CP cells

To gain further insight into the molecular properties of these two functionally distinct pools of epidermal progenitors, we transcriptionally profiled FACS-purified $\alpha6^{+}CD34^{-}$ K14-Cre-ER and Inv-Cre-ER YFP-positive IFE cells 3.5 days after tamoxifen administration (Supplementary Fig. 7). Comparison of the K14 and Inv transcriptome revealed notable differences. All markers previously associated with murine and human IFE SCs[25,27–29] were upregulated in K14-targeted cells, including α6, α2, α3, β1 integrins and *Cspg4* (Supplementary Fig. 8). Real-time quantitative reverse transcriptase-PCR (qRT–PCR) performed on independent biological samples confirmed the upregulation of these integrins in K14-targeted cells (Fig. 4a). FACS analysis showed that α6β4 integrins were expressed at a higher and more uniform level in K14- than in Inv-targeted cells. The pattern of α2β1 integrin showed a more notable difference between the two populations, with a very high and narrow peak of α2β1 expression in K14-targeted cells compared to the much lower and heterogeneous α2β1 expression in Inv-targeted cells (Fig. 4b, c and Supplementary Fig. 9). Gene ontology classification of the genes differentially expressed by more than 1.5-fold between K14- and Inv-labelled cells revealed that genes preferentially expressed in K14-positive cells are enriched with a very high statistical significance in functional groups involved in positive and negative cell cycle regulation (for example, *Ccnd2*, *Cdc20*, *Cdkn1a*, *Cdkn2a*), mitosis (for example, *Ccnb1*, *Kif11*), chromosome segregation (for example, *Cenpe*), regulation of cell proliferation (for example, *Epgn*), and DNA repair (for example, *Brca1*) (Fig. 4a, Supplementary Figs 8, 10a and Supplementary Table 1). By contrast, Inv-Cre-ER labelled cells preferentially expressed genes known to control epidermal differentiation[30–32] (for example, *Notch3*, *Grhl3*), keratinocyte differentiation and keratinization (for example, *Sppr1a*, *1b*, *2d*, *2i*)[33], and lipid metabolism (for example, *Elovl4*, *6*, *7*, *Olah*), as confirmed by qRT–PCR analysis (Fig. 4d, Supplementary Figs 8, 10b and Supplementary Table 1). Altogether these data demonstrate that K14- and Inv-targeted cells differ by their gene expression profile, and uncover many new markers preferentially expressed by IFE SC and CP cells.

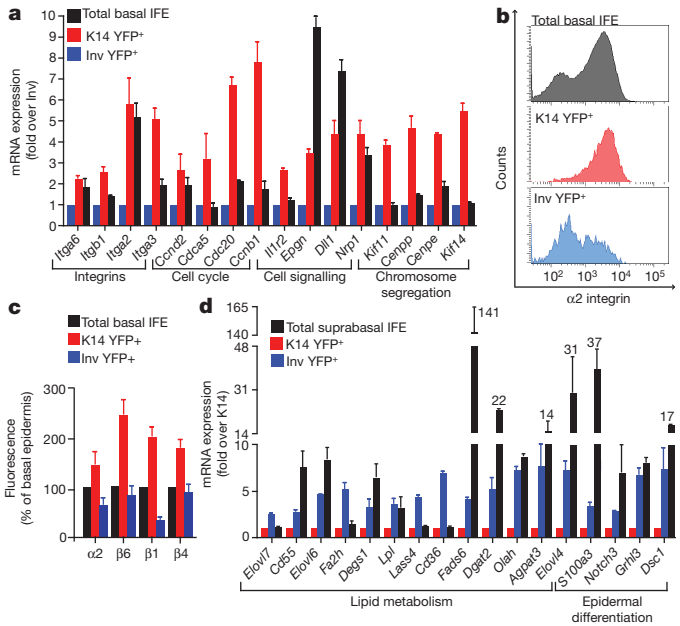

Figure 4 | Molecular signature of K14 SC and Inv CP cells. **a**, qRT–PCR analysis of the expression of representative genes upregulated in K14-Cre-ER-targeted cells, compared with the level of expression of the same genes in Inv-Cre-ER-targeted cells and total basal IFE cells ($n = 3$). **b**, **c**, Fluorescence histogram (**b**) and geometric mean fluorescence (**c**) of integrin cell-surface expression in all basal IFE cells, K14-Cre-ER- and Inv-Cre-ER-targeted IFE cells, as determined by FACS analysis, 3.5 days after tamoxifen ($n = 3$). **d**, qRT–PCR analysis of the expression of representative genes upregulated in Inv-Cre-ER-targeted cells, compared to the level of expression of the same genes in basal epidermal K14-Cre-ER-targeted cells and total suprabasal IFE cells ($n = 3$). Error bars show s.e.m.

To characterize further the molecular heterogeneity of basal IFE cells, we FACS-purified different populations of basal epidermal cells ($\alpha6^{+}CD34^{-}$) according to the level of β1 integrin expression which, together with α2 integrin, present the most significant difference between K14 and Inv-targeted cells at 3.5 days following tamoxifen administration (Fig. 4b and Supplementary Fig. 9). We fractionated epidermis into three distinct populations: one population (<3%) expressing very high levels of β1 integrin (which are likely to be enriched in SCs as they are only detected in K14- but not Inv-targeted cells), a second population expressing intermediate levels of β1 integrin detected in both K14 and Inv-targeted cells (which are likely to represent CP cells), and cells expressing low levels of β1 integrin only found in Inv-targeted cells (which are likely to represent the differentiated basal cells and early suprabasal cells) (Supplementary Fig. 11a). Strikingly, many markers identified as being upregulated in K14 versus Inv were also upregulated in cells expressing very high levels of β1 integrin compared to cells expressing intermediate or low levels (Supplementary Fig. 11b). Similarly, many genes preferentially expressed by Inv cells were already upregulated in cells expressing intermediate levels of β1 integrin compared to β1 integrin high cells but, nevertheless, much less expressed than in cells expressing low levels of β1 integrin (Supplementary Fig. 11c). These data demonstrate that the expression of many differentiation-associated genes is already upregulated at the earliest stage of progenitor commitment, reminiscent of the lineage priming reported in haematopoietic stem cells[34,35].

Long-term SC contribution to wound healing

In addition to their role in maintenance, adult SCs are implicated in the repair of damaged tissue following injury. Lineage tracing has shown that hair follicle SCs are mobilized to the wound area and contribute to the repair of damaged epidermis[15–18]. At the same time, genetic mouse mutants, that present a complete absence of hair follicle, heal incisional wounds with a slight delay of the reepithelialisation, demonstrating that IFE cells are also capable of tissue regeneration[36]. However, in unperturbed conditions, the contribution of IFE SCs and progenitors to wound healing is currently unknown. To address the respective contributions of K14-SCs and Inv-CPs during tissue repair, we first marked basal progenitors by titrating the dose of tamoxifen so as to label Inv and K14-Cre-ER epidermis at roughly the same density (4.5 ± 0.1 clones per mm^2 and 3.8 ± 0.5 clones per mm^2 in K14 and Inv, respectively), then subjected tail epidermis to full thickness excisional wound using punch biopsy, and assessed the contribution of marked cells to repair (Fig. 5a). Whole-mount analysis showed major recruitment of K14-Cre-ER-labelled IFE cells to the wound area, with clones migrating from the periphery towards the centre of the wound (with only 7.5% of clones from hair follicle), persisting long-term after wounding (2.6 ± 0.1 clones per mm^2 after 35 days) (Fig. 5b, c and Supplementary Fig. 12), and consisting of very large clones with a broad basal attachment and huge numbers of differentiated cells (Fig. 5d). In sharp contrast, few Inv-Cre-ER-targeted cells were recruited to the wound area, and these clones were, on average, much

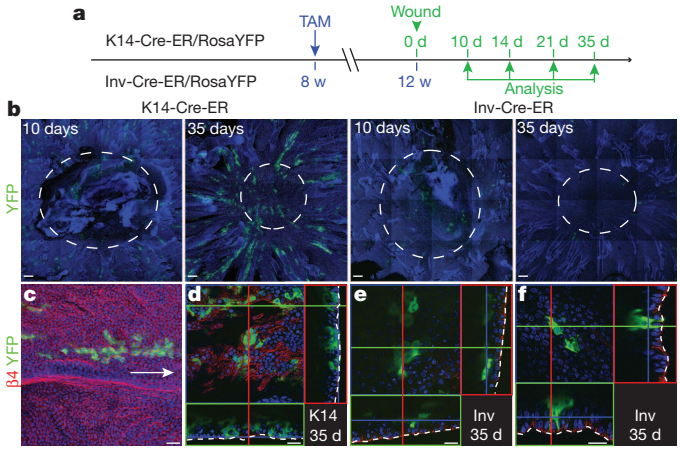

Figure 5 | Massive and sustained contribution of K14 SC during wound healing. **a**, Scheme representing the experimental strategy used to label basal progenitors and assess their contribution during wound healing. **b**, Microscopic analysis of YFP immunostaining performed on whole-mount of wounded tail epidermis 4 weeks after tamoxifen administration to K14-Cre-ER/RosaYFP and Inv-Cre-ER/RosaYFP mice and analysed at different times following wounding. Dashed lines represent the wounded area. Scale bar, 200 μm. **c**, Confocal analysis of whole-mount immunostaining of YFP and β4 integrin 21 days following wounding, showing the departure of K14 YFP labelled from the IFE. The arrow indicates the wound localization. Scale bars, 20 μm. **d**–**f**, Confocal analysis of representative clones from wounded tail epidermis 35 days post-wound, showing very big clones containing multiple basal cells in K14 targeted cells (**d**), whereas the rare still visible Inv marked clones are either completely detached from the basal epidermis (**e**) or very small containing one or few basal cells (**f**). Dashed lines represent the basal lamina. Scale bars, 20 μm. Hoechst nuclear staining is represented in blue.

smaller. At 35 days post-injury, few Inv clones survived (0.3 ± 0.3 clones per mm^2) and consisted of either clones of cells being shed with no basal attachment (Fig. 5e), or small clones with one or few basal cells (Fig. 5f). These data demonstrate that K14-derived SC are capable of extensive tissue regeneration, whereas Inv CP cells have only a limited contribution to wound healing.

Discussion

Our study demonstrates the existence, hierarchical organization and the proliferation dynamics of two distinct types of progenitors that effect different functions during homeostasis and repair of the IFE in adult mice. Quantitative modelling of clonal fate data suggest that both the slow-cycling SCs and the more rapidly cycling CP cells share a similar pattern of population asymmetric self-renewal in which the balance between proliferation and differentiation is achieved through stochastic fate choice (Supplementary Fig. 13). These findings provide a reconciliation of seemingly contradictory theories of IFE maintenance[4,12], and explain the proliferative heterogeneity previously reported in IFE[5,37,38]. The existence of slow-cycling SCs and more rapidly cycling progenitors is reminiscent of the situation encountered in other tissues including cornea[39], hair follicle[40], blood[41,42], muscle[43] and brain[44]. In all of these tissues, these slow-cycling SCs can switch rapidly and reversibly between quiescence and activity following injury and/or drug treatment[15,45]. Indeed, this partitioning of function—progenitors to undertake routine maintenance and quiescent SCs to effect repair—may represent a generic strategy of tissue maintenance.

The demonstration that the long-term wound healing potential is dominated by the IFE SC compartment may suggest that either SC and CP cell populations are not interchangeable, in contrast to progenitors in intestinal epithelium[46], or that their reversion rate is sufficiently slow to render its effects negligible. The seemingly short-lived contribution of Inv CP cells to the repair of the epidermis is reminiscent of the fate of K15 bulge-derived SCs during wounding[16], and demonstrates the critical role of IFE SCs for the long-term repair of the epidermis, as has been proposed[16].

METHODS SUMMARY

Clonal YFP expression in the tail IFE was performed by administrating 0.2 mg and 2.5 mg tamoxifen to K14-Cre-ER/RosaYFP and Inv-Cre-ER/RosaYFP mice, respectively. Immunostainings were performed as described[47]. Quantification of the proportion of surviving clones as well as the basal, suprabasal and total clone size was determined by counting the number of YFP^+ cells using whole-mount tail epidermis, analysed by confocal microscopy. BrdU pulse and H2B–GFP label retention was performed as described[15,43]. The wound healing assay was performed by administrating 1 mg and 10 mg tamoxifen to K14-Cre-ER/RosaYFP and Inv-Cre-ER/RosaYFP mice, respectively. Four weeks later punch biopsies were performed in the tail epidermis and analysed at different time points. Mathematical modelling of the clonal fate data was performed as described in Supplementary Methods, section 'Theory'. For further details see Supplementary Methods.

Full Methods and any associated references are available in the online version of the paper.

Received 13 March; accepted 3 July 2012.
Published online 2 September 2012.

1. Blanpain, C. & Fuchs, E. Epidermal homeostasis: a balancing act of stem cells in the skin. *Nature Rev. Mol. Cell Biol.* **10,** 207–217 (2009).
2. Potten, C. S., Saffhill, R. & Maibach, H. I. Measurement of the transit time for cells through the epidermis and stratum corneum of the mouse and guinea-pig. *Cell Tissue Kinet.* **20,** 461–472 (1987).
3. Potten, C. S. Cell replacement in epidermis (keratopoiesis) via discrete units of proliferation. *Int. Rev. Cytol.* **69,** 271–318 (1981).
4. Potten, C. S., Wichmann, H. E., Loeffler, M., Dobek, K. & Major, D. Evidence for discrete cell kinetic subpopulations in mouse epidermis based on mathematical analysis. *Cell Tissue Kinet.* **15,** 305–329 (1982).
5. Potten, C. S. & Loeffler, M. Epidermal cell proliferation. I. Changes with time in the proportion of isolated, paired and clustered labelled cells in sheets of murine epidermis. *Virchows Arch. B Cell Pathol. Incl. Mol. Pathol.* **53,** 279–285 (1987).
6. Mackenzie, I. C. Retroviral transduction of murine epidermal stem cells demonstrates clonal units of epidermal structure. *J. Invest. Dermatol.* **109,** 377–383 (1997).
7. Kolodka, T. M., Garlick, J. A. & Taichman, L. B. Evidence for keratinocyte stem cells *in vitro*: long term engraftment and persistence of transgene expression from retrovirus-transduced keratinocytes. *Proc. Natl Acad. Sci. USA* **95,** 4356–4361 (1998).
8. Ghazizadeh, S. & Taichman, L. B. Multiple classes of stem cells in cutaneous epithelium: a lineage analysis of adult mouse skin. *EMBO J.* **20,** 1215–1222 (2001).
9. Ghazizadeh, S. & Taichman, L. B. Organization of stem cells and their progeny in human epidermis. *J. Invest. Dermatol.* **124,** 367–372 (2005).
10. Ro, S. & Rannala, B. A stop-EGFP transgenic mouse to detect clonal cell lineages generated by mutation. *EMBO Rep.* **5,** 914–920 (2004).
11. Ro, S. & Rannala, B. Evidence from the stop-EGFP mouse supports a niche-sharing model of epidermal proliferative units. *Exp. Dermatol.* **14,** 838–843 (2005).
12. Clayton, E. *et al.* A single type of progenitor cell maintains normal epidermis. *Nature* **446,** 185–189 (2007).
13. Doupé, D. P., Klein, A. M., Simons, B. D. & Jones, P. H. The ordered architecture of murine ear epidermis is maintained by progenitor cells with random fate. *Dev. Cell* **18,** 317–323 (2010).
14. Jones, P. & Simons, B. D. Epidermal homeostasis: do committed progenitors work while stem cells sleep? *Nature Rev. Mol. Cell Biol.* **9,** 82–88 (2008).
15. Tumbar, T. *et al.* Defining the epithelial stem cell niche in skin. *Science* **303,** 359–363 (2004).
16. Ito, M. *et al.* Stem cells in the hair follicle bulge contribute to wound repair but not to homeostasis of the epidermis. *Nature Med.* **11,** 1351–1354 (2005).
17. Levy, V., Lindon, C., Zheng, Y., Harfe, B. D. & Morgan, B. A. Epidermal stem cells arise from the hair follicle after wounding. *FASEB J.* **21,** 1358–1366 (2007).
18. Snippert, H. J. *et al. Lgr6* marks stem cells in the hair follicle that generate all cell lineages of the skin. *Science* **327,** 1385–1389 (2010).
19. Vasioukhin, V., Degenstein, L., Wise, B. & Fuchs, E. The magical touch: genome targeting in epidermal stem cells induced by tamoxifen application to mouse skin. *Proc. Natl Acad. Sci. USA* **96,** 8551–8556 (1999).
20. Lapouge, G. *et al.* Identifying the cellular origin of squamous skin tumors. *Proc. Natl Acad. Sci. USA* **108,** 7431–7436 (2011).
21. Klein, A. M. & Simons, B. D. Universal patterns of stem cell fate in cycling adult tissues. *Development* **138,** 3103–3111 (2011).
22. Waghmare, S. K. *et al.* Quantitative proliferation dynamics and random chromosome segregation of hair follicle stem cells. *EMBO J.* **27,** 1309–1320 (2008).
23. Zhang, Y. V., Cheong, J., Ciapurin, N., McDermitt, D. J. & Tumbar, T. Distinct self-renewal and differentiation phases in the niche of infrequently dividing hair follicle stem cells. *Cell Stem Cell* **5,** 267–278 (2009).
24. Zhang, Y. V., White, B. S., Shalloway, D. I. & Tumbar, T. Stem cell dynamics in mouse hair follicles: A story from cell division counting and single cell lineage tracing. *Cell Cycle* **9,** 1504–1510 (2010).

25. Jones, P. H., Harper, S. & Watt, F. M. Stem cell patterning and fate in human epidermis. *Cell* **80,** 83–93 (1995).
26. Lavker, R. M. & Sun, T. T. Heterogeneity in epidermal basal keratinocytes: morphological and functional correlations. *Science* **215,** 1239–1241 (1982).
27. Jones, P. H. & Watt, F. M. Separation of human epidermal stem cells from transit amplifying cells on the basis of differences in integrin function and expression. *Cell* **73,** 713–724 (1993).
28. Legg, J., Jensen, U. B., Broad, S., Leigh, I. & Watt, F. M. Role of melanoma chondroitin sulphate proteoglycan in patterning stem cells in human interfollicular epidermis. *Development* **130,** 6049–6063 (2003).
29. Tani, H., Morris, R. J. & Kaur, P. Enrichment for murine keratinocyte stem cells based on cell surface phenotype. *Proc. Natl Acad. Sci. USA* **97,** 10960–10965 (2000).
30. Rangarajan, A. *et al.* Notch signaling is a direct determinant of keratinocyte growth arrest and entry into differentiation. *EMBO J.* **20,** 3427–3436 (2001).
31. Blanpain, C., Lowry, W. E., Pasolli, H. A. & Fuchs, E. Canonical notch signaling functions as a commitment switch in the epidermal lineage. *Genes Dev.* **20,** 3022–3035 (2006).
32. Ting, S. B. *et al.* A homolog of *Drosophila* grainy head is essential for epidermal integrity in mice. *Science* **308,** 411–413 (2005).
33. Candi, E., Schmidt, R. & Melino, G. The cornified envelope: a model of cell death in the skin. *Nature Rev. Mol. Cell Biol.* **6,** 328–340 (2005).
34. Månsson, R. *et al.* Molecular evidence for hierarchical transcriptional lineage priming in fetal and adult stem cells and multipotent progenitors. *Immunity* **26,** 407–419 (2007).
35. Pina, C. *et al.* Inferring rules of lineage commitment in haematopoiesis. *Nature Cell Biol.* **14,** 287–294 (2012).
36. Langton, A. K., Herrick, S. E. & Headon, D. J. An extended epidermal response heals cutaneous wounds in the absence of a hair follicle stem cell contribution. *J. Invest. Dermatol.* **128,** 1311–1318 (2008).
37. Loeffler, M., Potten, C. S. & Wichmann, H. E. Epidermal cell proliferation. II. A comprehensive mathematical model of cell proliferation and migration in the basal layer predicts some unusual properties of epidermal stem cells. *Virchows Arch. B Cell Pathol. Incl. Mol. Pathol.* **53,** 286–300 (1987).
38. Morris, R. J., Fischer, S. M. & Slaga, T. J. Evidence that the centrally and peripherally located cells in the murine epidermal proliferative unit are two distinct cell populations. *J. Invest. Dermatol.* **84,** 277–281 (1985).
39. Cotsarelis, G., Cheng, S. Z., Dong, G., Sun, T. T. & Lavker, R. M. Existence of slow-cycling limbal epithelial basal cells that can be preferentially stimulated to proliferate: implications on epithelial stem cells. *Cell* **57,** 201–209 (1989).
40. Cotsarelis, G., Sun, T. T. & Lavker, R. M. Label-retaining cells reside in the bulge area of pilosebaceous unit: implications for follicular stem cells, hair cycle, and skin carcinogenesis. *Cell* **61,** 1329–1337 (1990).
41. Wilson, A. *et al.* Hematopoietic stem cells reversibly switch from dormancy to self-renewal during homeostasis and repair. *Cell* **135,** 1118–1129 (2008).
42. Foudi, A. *et al.* Analysis of histone 2B-GFP retention reveals slowly cycling hematopoietic stem cells. *Nature Biotechnol.* **27,** 84–90 (2009).
43. Rocheteau, P., Gayraud-Morel, B., Siegl-Cachedenier, I., Blasco, M. A. & Tajbakhsh, S. A subpopulation of adult skeletal muscle stem cells retains all template DNA strands after cell division. *Cell* **148,** 112–125 (2012).
44. Bonaguidi, M. A. *et al. In vivo* clonal analysis reveals self-renewing and multipotent adult neural stem cell characteristics. *Cell* **145,** 1142–1155 (2011).
45. Essers, M. A. *et al.* IFNα activates dormant haematopoietic stem cells *in vivo*. *Nature* **458,** 904–908 (2009).
46. Takeda, N. *et al.* Interconversion between intestinal stem cell populations in distinct niches. *Science* **334,** 1420–1424 (2011).
47. Youssef, K. K. *et al.* Identification of the cell lineage at the origin of basal cell carcinoma. *Nature Cell Biol.* **12,** 299–305 (2010).

Supplementary Information is available in the online version of the paper.

Acknowledgements We thank F. Bollet-Quivogne and J.-M. Vanderwinden for their help with confocal imaging. C.B. and P.A.S. are chercheur qualifié, G.M. and S.B. are supported by fellowship of the FRS/FNRS. B.D. is supported by TELEVIE. C.B. is an investigator of WELBIO. This work was supported by the FNRS, the program d'excellence CIBLES of the Wallonia Region, a research grant from the Fondation Contre le Cancer, the ULB fondation, the fond Gaston Ithier, the European Research Council (ERC) and the EMBO Young Investigator Program.

Author Contributions C.B., G.M., B.D., S.D., P.A.S. and B.D.S. designed the experiments and performed data analysis. G.M., S.D., B.D. and K.K.Y. performed all the experiments. S.B. performed bioinformatic analysis of the microarray. C.B. and B.D.S. wrote the manuscript.

Author Information The data discussed in this publication have been deposited in the NCBI Gene Expression Omnibus and are accessible through GEO Series accession number GSE36688. Reprints and permissions information is available at www.nature.com/reprints. The authors declare no competing financial interests. Readers are welcome to comment on the online version of the paper. Correspondence and requests for materials should be addressed to C.B. (cedric.blanpain@ulb.ac.be) or B.D.S. (bds10@cam.ac.uk).

METHODS

Mice. K14-Cre-ER[19] and TRE-mCMV-H2B-GFP[15] transgenic mice were provided by E. Fuchs. K5-tTA mice[48] were a gift from A. Glick. RosaYFP mice[49] were obtained from Jackson Laboratory. Involucrin-CreERT2 were previously described[20]. Mouse colonies were maintained in a certified animal facility in accordance with European guidelines. These experiments were approved by the local ethical committee (CEBEA).

Targeting YFP expression. For lineage tracing experiment, K14-Cre-ER/RosaYFP and Involucrin-CRERT2/Rosa-YFP mice were induced between 2 and 4 months with 0.2 mg and 2.5 mg of tamoxifen (Sigma-Aldrich), respectively, by intraperitoneal injection.

For cell sorting, K14-Cre-ER/RosaYFP and Inv-Cre-ER/RosaYFP mice were induced with 1 mg and 10 mg of tamoxifen, respectively, by intraperitoneal injection and isolated 4 days later.

Proliferation experiments. For H2B–GFP chase, K5-Tet off /TRE-mCMV-H2B-GFP were treated once with 200 µl of doxycycline (2 mg ml^{-1}) by intraperitoneal injection and simultaneously continually fed with doxycycline food (1 g kg^{-1}) until animal euthanasia. For BrdU experiment, mice were injected every 12 h with 200 µl of BrdU (10 mg ml^{-1}) and analysed 24 h and 72 h after the first injection.

Wound experiments. After mice anaesthesia (5% xylazine 10% ketamine in PBS), circular pieces of epidermis were removed from K14-Cre-ER/Rosa YFP and Inv-Cre-ER/RosaYFP tail epidermis, 4 weeks after tamoxifen induction, using a 3 mm diameter biopsy punch (Stiefel).

Histology and immunostaining. Skin epidermis was removed from tail bone and pre-fixed overnight in 4% paraformaldehyde at 4 °C. Tissues were washed three times in PBS for 5 min and incubated overnight in 30% sucrose in PBS at 4 °C. Tissues were then embedded in OCT and kept at −80 °C. Sections of 6 µm were cut using a CM3050S Leica cryostat (Leica Mycrosystems).

Sections were incubated in blocking buffer (1% BSA, 5% horse serum, 0.2% Triton in PBS) for 1 h at room temperature. Primary antibodies were incubated overnight at 4 °C or 1 h at room temperature in the dark. Sections were rinsed three times in PBS and incubated with appropriate secondary antibodies diluted to 1:400 and Hoeschst in blocking buffer for 1 h at room temperature. Sections were again washed three times with PBS. The following primary antibodies were used: anti-involucrin (rabbit, 1:1,000, Covance), anti-K5 (rabbit, 1:1,000, Covance), anti-K10 (rabbit, 1:1,000, Covance), anti-β4 (rat, 1:200, BD Biosciences), anti-GFP (rabbit, 1:1,000, Molecular Probes), anti-GFP (chicken, 1:1,000, Abcam). The following secondary antibodies were used: anti-rabbit, anti-rat, anti-goat, anti-chicken conjugated to Alexa Fluor 488 (Molecular Probes), to rhodamine Red-X (Jackson Immunoresearch) or to Cy5 (Jackson Immunoresearch). Nuclei were stained in Hoechst solution (1:2,000) and slides were mounted in DAKO mounting medium supplemented with 2.5% Dabco (Sigma).

Epidermal whole-mount. Pieces of skin tail were incubated in EDTA (20 mM) on a rocking plate at 37 °C for 1 h. Epidermis was separated from the dermis as an intact sheet and washed 2 times with PBS. Pieces of epidermis were pre-fixed in 4% paraformaldehyde overnight at 4 °C or 1 h at room temperature. Epidermis were rinsed 2 times with PBS for 5 min and conserved in PBS with 0.2% azide at 4 °C. Small pieces of epidermis were incubated in blocking buffer (1% BSA, 5% horse serum, 0.8% Triton in PBS) for 3 h at room temperature on a rocking plate (100 r.p.m.). The samples were incubated in primary antibodies overnight at room temperature on the rocking plate. The primary antibodies used were the following: anti-K5 (rabbit, 1:200, Covance), anti-β4 (rat, 1:100, BD Biosciences), anti-GFP (rabbit, 1:200, Molecular Probes), anti-GFP (chicken, 1:200, Abcam). Samples were then washed 3 times in PBS with 0.2% tween for 1 h and incubated in appropriate secondary antibodies diluted 1:400 in blocking buffer overnight at 4 °C on the rocking plate. Pieces of epidermis were then washed with PBS 3 times for 1 h. For BrdU staining, samples were incubated in HCl 1 M at 37 °C for 20 min, washed with PBS 0,2% tween, stained with anti-BrdU (rat, 1:200, Abcam) in blocking buffer and with appropriate secondary antibody after several washes. Nuclei were stained in Hoechst solution diluted 1:1,000 for 30 min and mounted in DAKO mounting medium supplemented with 2.5% Dabco (Sigma).

TPA experiment. 12-*O*-tetradecanoyl-phorbol-13-acetate (TPA) from Sigma has been diluted in acetone (final concentration 25 mg ml^{-1}). K14-Cre-ER/RosaYFP mice were topically treated with TPA on tail epidermis during 11 days, induced with tamoxifen the 8th days. The 12th day, treated mice were killed and processed to get whole-mounts of tail epidermis.

Microscope image acquisition and quantification. All pictures of section immunostaining were acquired using the Axio Imager M1 Microscope, the AxioCamMR3 or MrC5 camera and using the Axiovision software (Carl Zeiss). Acquisitions were performed at room temperature using ×20 numerical aperture (NA) 0.4 and ×40 NA 0.75 EC Plan-Neofluar objectives (Carl Zeiss). All confocal pictures on whole-mount were acquired at room temperature using a Zeiss LSM780 confocal microscope fitted on an Axiovert M200 inverted microscope equipped with a ×40 NA 1.2 C-Apochromat water immersion objective (Carl Zeiss MicroImaging GmbH). Sequential scannings of 1,024 × 1,024 pixels, *z*-stack 0.3 µm, were acquired using the ZEN 2010 software (Carl Zeiss).

Number of basal clones per interfollicular region were quantified on frozen section using Axio Imager M1 microscope for each time point and represented as percentage of basal clone. Clone sizes were quantified on whole-mount tail epidermis by acquiring individual clones using LSM 780 confocal microscope and the number of basal and suprabasal cells were counted.

Dissociation of epidermal cells. Skin epidermis (from CD1, K5tTA/tet(o)-H2BGFP treated or not with DOX, K14-Cre-ER and Inv-Cre-ER/RosaYFP induced with tamoxifen for 3.5 days or 8 weeks) was removed from tail bone and incubated overnight in HBSS (Gibco) 0.25% trypsin (Gibco) at 4 °C. Epidermis was separated from the dermis and incubated on a rocking plate (100 r.p.m.) at room temperature for 5 min. Basal cells were mechanically separated from the epidermis by flushing 10 times under the epidermis. Tissues were then cut in pieces of 1 mm^2 with scalpel and trypsin was neutralized by adding DMEM medium (Gibco) supplemented with 2% Chelex fetal calf serum (FCS). Samples were filtrated on 70- and 40-µm filter (Falcon).

Cell labelling, flow cytometry and cell sorting. Using a concentration of 20 millions cells per ml, cells were incubated in 2% FCS/PBS with primary antibodies for 30 min on ice, protected from the light, with shaking every 10 min. Immunostaining for isolating K14 and involucrin cells was performed using biotin-conjugated anti-CD34 (clone RAM34; BD Biosciences) and phycoerythrin-conjugated anti-α6 integrin (clone GoH3; BD biosciences). Primary antibodies were washed with 2% FCS/PBS and cells incubated for 30 min in allophycocyanin-conjugated streptavidin (BD Biosciences) secondary antibodies, on ice, with shaking every 10 min. Living K14 and involucrin expressing epidermal cells were gated by forward scatter, side scatter, negative staining for Hoechst dye and by following the YFP signal. Basal cells from the interfollicular epidermis were targeted using CD34-negative α6-integrin-positive gating. Immunostaining for isolating basal β1 high, intermediate and low cells was performed using biotin-conjugated anti-CD34 revealed with a phycoerythrin-Cy7-conjugated streptavidin (BD Biosciences) and anti-CD29 allophycocyanin-conjugated (β1 integrin, clone Hmb1-1, eBiosciences). Single living, CD34-negative, β1 low/medium/high cells were sorted. β1 low, medium and high gates were set up on the basis of its expression in K14-Cre-ER- and Inv-Cre-ER/RosaYFP-targeted basal IFE cells. Fluorescence-activated cell sorting analysis was performed using FACSAria I at high pressure (70 p.s.i.) and FACSDiva software (BD Biosciences). Sorted cells were harvested directly in the lysis buffer provided by the RNeasy microkit (QIAGEN) supplemented with 1 µl of beta-mercaptoethanol for every 100 µl of lysis buffer. RNA extraction was performed on freshly sorted cells according to the manufacturer's protocol. The entire procedure was repeated in at least three biologically independent samples. Other integrin antibodies were used to determine their expression in the different cell populations: anti-CD49b phycoerythrin-conjugated (α2 integrin, clone Hmα2, BD biosciences), anti-CD29 allophycocyanin-conjugated, and anti-CD104 rat (β4 integrin, clone 346 11A, BD Biosciences) revealed with an anti-rat Rhodamine Red x-conjugated (donkey, JacksonImmunoResearch).

Total suprabasal and total basal IFE cells isolation for qPCR controls. For total suprabasal IFE control, skin epidermis was removed from tail bone and incubated 1 h in EDTA (20 mM) on a rocking plate at 37 °C. Epidermis was separated from the dermis and basal cells were flushed out from the epidermis. The piece of epidermis containing the suprabasal cells was then frozen in liquid nitrogen. RNA extraction was performed using RNeasy microkit (QIAGEN): the tissue was cut in small pieces and lysed in RLT buffer containing β-mercaptoethanol according to the manufacturer's protocol. For total basal IFE qPCR control, cells were obtained by gating the whole $\alpha6^+$ (low medium and high) and $CD34^-$ population in FACS sorting.

RNA quality. Extracted RNA quality was tested using capillary electrophoresis (Agilent Bioanalyzer, Agilent RNA 6000 Nano Kit). Degraded RNA samples or presenting sign of degradation or containing high proteins or salt contamination were discarded.

Microarray analysis. Cohort of 10 Inv-Cre-ER/RosaYFP and K14-Cre-ER/RosaYFP mice were used to isolate at least 100,000 basal IFE cells ($\alpha6^+$ $CD34^-$ YFP^+) per replicate. Total RNAs were isolated from these sorted cells and were labelled and hybridized on a mouse genome 430 2.0 array. Microarrays were performed in duplicate for the untreated K14-Cre-ER/RosaYFP and tamoxifen-treated K14-Cre-ER/RosaYFP and Inv-Cre-ER/RosaYFP sorted cells. All the results were normalized using the frozen robust multiarray analysis (fRMA) normalization using R-bioconductor package fRMA[50,51] with standard parameters. Genetic signatures were obtained by considering genes presenting a fold change greater on smaller than 2 or −2, respectively.

Reverse transcription and quantitative PCR. Cohort of 10 Inv-Cre-ER/RosaYFP and K14-Cre-ER/RosaYFP mice were used to isolate at least 100,000 basal IFE cells ($\alpha6^+$ $CD34^-$ YFP^+) per replicate. Each RNA sample was quantified using a nanodrop spectrophotometer. RNA quality and quantity used for qRT–PCR was exactly the same as for the RNA used for Microarray analysis. Purified RNA (200 ng) was used to synthesize the first-strand cDNA using Superscript II (Invitrogen) and random hexamers (Roche). Mock was obtained following the same procedure without adding Superscript II. Quantitative PCR analyses were performed with 1 ng of complementary DNA as template, using a Brilliant II Fast SYBR QPCR Master Green mix (Stratagene) and an Agilent Technologies Stratagene Mx3500P real-time PCR system.

All primers were designed using the Assay Design Center (Roche applied science, https://www.roche-applied-science.com/sis/rtpcr/upl/index.jsp?id=uplct_030000). The list of primers are shown in the table underneath. The linearity of each pair of primer used has been tested with the following dilution of cDNA: 8 ng, 2 ng, 0.5 ng, 0.125 ng.

Analysis of results was performed with Mxpro software (Stratagene). Delta delta CT were used to calculate the relative expression of involucrin samples to the K14 samples using the housekeeping gene TataBox.

Primers. Gene symbol, forward primer and reverse primer (5′ to 3′) are: *Agpat3*, ccatcagcaagcacctatacc and cactccaggagcatgacca;*Ccnb1*, tgcattttgctccttctcaa and caggaagcagggagtcttca; *Ccnd2*, caccgacaactctgtgaagc and tccacttcagcttacccaaca; *Cd36*, ttgtacctatactgtggctaaatgaga and cttgtgttttgaacatttctgctt; *Cd55*, actgttgattggg acgatgag and tggtggctctggacaatgta; *Cdc20*, acatcaaggcgctgtcaag and aatgtgccggtc actggt; *Cdca5*, cacagtgacttatgtaggaactggtc and caccccgttcaccaatgt; *Cenpe*, tctttaccgtctgaggtggaa and ggagctcttcagatttctcataca; *Cenpp*, gcagaatgctgcaaaacg and caaagattcccactcctcaga; *Degs1*, tcaccttcaatgtgggctatc and cacttgcgatcttcctcacc; *Dgat2*, ggcgctacttccgagactac and tggtcagcaggttgtgtgtc; *Dll1*, gggcttctctggcttcaac and taagagttgccgaggtccac; *Dsc1*, gggagcaccttctctaagca and ttttgacaggcatcacaaaat aa; *Elovl4*, acgacaccgtggagttctatc and gcggccagtctgctacac; *Elovl6*, cagcaaagcacccg aacta and aggagcacagtgatgtggtg; *Elovl7*, tctcagtcgccaagagcaa and acagctcgatga atttggaga; *Epgn*, ggctctgggggttctgatag and cctctgcttcttcgctcagt; *Fa2h*, tggtggactggg acaagg and gttggtgaacccactcatca; *Fads6*, ccacccttatctccatgtcaa and cttgtccggggag aacatag; *Grhl3*, aaggaagatgtcgaatgaacttg and tcgtcctcattactgtagggaaa; *Il1r2*, cccatccctgtgatcatttc and gcacgggactatcagtcttga; involucrin, atgtcccatcaacacacactg and atgtcccatcaacacacactg; *Itga2*, gggaccggaggctttcta and tgcataatactgatttccacactg; *Itga3*, aggatatgtggcttggagtga and gaccacagcaccttggtgta; *Itga6*, attcaggagtagcttggtg gat and cttatttctcttgaagaagccacac; *Itgb1*, atgcaggttgcggtttgt and catccgtggaaaacacc ag; *Kif11*, aaagaggaaaagggcaggaa and ccgctctgccagattaaatg; *Kif14*, ggctatttgcaat tgtttttgc and tttgagcctctttaaccatcg; *Kif2c*, cgaaggaggtaccacaaaagg and ttcggtc gtaagggaagaag; *Lass4*, gcctgcatcttgctttctg and ctgccacagccactcactc; *Lpl*, ctggt gggaaatgatgtgg and tggacgttgtctaggggga; *Notch3*, agctgggtcctgaggtgat and agacag agccggttgtcaat; *Nrp1*, gaggaatgttctgtcgctatga and ccaatgtgagggccaact; *Olah*, ggccgaaagattaatggctta and ggttcttcaaatcgggtttct; *S100a3*, gggacacccagttggtagg and gcacacgatggcagctact; T-box, gtaccgcagcttcaaaatattgtat and aaatcaacgcag ttgtgcgtg.

48. Diamond, I., Owolabi, T., Marco, M., Lam, C. & Glick, A. Conditional gene expression in the epidermis of transgenic mice using the tetracycline-regulated transactivators tTA and rTA linked to the keratin 5 promoter. *J. Invest. Dermatol.* **115,** 788–794 (2000).
49. Srinivas, S. *et al.* Cre reporter strains produced by targeted insertion of *EYFP* and *ECFP* into the *ROSA26* locus. *BMC Dev. Biol.* **1,** 4 (2001).
50. Gentleman, R. C. *et al.* Bioconductor: open software development for computational biology and bioinformatics. *Genome Biol.* **5,** R80 (2004).
51. McCall, M. N., Bolstad, B. M. & Irizarry, R. A. Frozen robust multiarray analysis (fRMA). *Biostatistics* **11,** 242–253 (2010).